

Star formation in the hosts of GHz peaked spectrum and compact steep spectrum radio galaxies

A. Labiano^{1,2}, C. P. O’Dea³, P. D. Barthel², W. H. de Vries^{4,5}, and S.A. Baum⁶

¹ Departamento de Astrofísica Molecular e Infrarroja, Instituto de Estructura de la Materia (CSIC), Madrid, Spain

² Kapteyn Astronomical Institute, Groningen, 9700 AV, The Netherlands

³ Department of Physics, Rochester Institute of Technology, Rochester, NY, 14623, USA

⁴ University of California, Davis, CA 95616, USA

⁵ Lawrence Livermore National Laboratory, IGPP, Livermore, CA 94550, USA

⁶ Center for Imaging Science, Rochester Institute of Technology, Rochester, NY 14623. USA

ABSTRACT

Aims. Search for star formation regions in the hosts of potentially young radio galaxies (Gigahertz Peaked Spectrum and Compact Steep Spectrum sources).

Methods. Near-UV imaging with the Hubble Space Telescope Advanced Camera for Surveys.

Results. We find near-UV light which could be the product of recent star formation in eight of the nine observed sources, though other explanations are not currently ruled out. The UV luminosities of the GPS and CSS sources are similar to those of a sample of nearby large scale radio galaxies. Stellar population synthesis models are consistent with a burst of recent star formation occurring before the formation of the radio source. However, observations at other wavelengths and colors are needed to definitively establish the nature of the observed UV light. In the CSS sources 1443+77 and 1814–637 the near-UV light is aligned with and is co-spatial with the radio source. We suggest that in these sources the UV light is produced by star formation triggered and/or enhanced by the radio source.

Key words. Galaxies: active – Galaxies: starburst – Galaxies: evolution – Galaxies: stellar content – Galaxies: interaction – Ultraviolet: galaxies

1. Introduction

The relationship between black hole mass and galaxy mass implies that the growth and evolution of black holes (therefore AGN) and their host galaxies must somehow be related (e.g., Gebhardt et al. 2000). Mergers and strong interactions can trigger AGN activity in a galaxy (e.g., Heckman et al. 1986; Baum et al. 1992; Israel 1998). These events can also produce instabilities in the ISM and trigger star formation (e.g., Ho 2005). Numerical simulations and models (e.g., Mellema et al. 2002; Rees 1989) suggest that the advancement of the jets through the host galaxy environment can also trigger star formation. Imaging studies in the ultraviolet (UV) light of large 3CR sources find evidence for episodes of star formation starting around the time when the radio source was triggered (i.e. $\lesssim 10^7 - 10^8$ yr, Koekemoer et al. 1999; Allen et al. 2002; Chiaberge et al. 2002; O’Dea et al. 2001, 2003; Martel et al. 2002) suggesting a possible link.

Gigahertz Peaked Spectrum (GPS) and Compact Steep Spectrum (CSS) radio sources are apparently young, smaller (GPS $\lesssim 1$ kpc, CSS $\lesssim 15$ kpc, for a review see O’Dea 1998) versions of the large powerful radio sources, so they are expected to exhibit signs of more recent star formation. In addition, their subgalactic size makes them excellent probes of the interactions between the expanding lobes and the host. They have not completely broken through the host ISM, so these interactions are expected to be more important than in the larger sources.

Near UV observations are very sensitive to the presence of hot young stars and as such will trace recent star formation events. We have therefore obtained high resolution HST/ACS near-UV images of these young compact sources to study the morphology and the extent of recent star formation.

This is the first time a sample of GPS and CSS sources has been imaged in the near-UV. It is also the first time that the relative sizes of radio sources in well matched samples are used to study time evolution of merger-induced and jet-induced star formation.

2. Observations and data reduction

We have obtained high resolution near-UV images with the High Resolution Channel (HRC) of the Advanced Camera for surveys (ACS) on board the Hubble Space Telescope, through the F330W filter. The objects observed are GPS and CSS galaxies 1117+146, 1233+418, 1345+125, 1443+77, 1607+268, 1814–637, 1934–638, 1946+708, 2352+495 (Table 1). Our sample is chosen to be representative of GPS and CSS sources with $z \leq 0.5$, and nearby enough to eliminate strong effects due to evolution with cosmic time. The objects are drawn primarily from the well-defined samples of Fanti et al. (1990), Fanti et al. (2001), Stanghellini (1992) and Stanghellini et al. (1997). The comparison sample of large 3CR sources consists of FR I and FR II sources with redshifts less than 0.1 observed in the near-UV by Allen et al. (2002).

The standard ACS reduction pipeline was used to remove detector signatures such as bias, dark current, flat field and to perform flux calibration. Each target was observed in a two-point dither pattern. The frames were combined with Multidrizzle (Koekemoer et al. 2002) to correct for geometric distortions and cosmic rays. The resulting ACS images have a signal to noise of ~ 100 for the brightest objects and ~ 5 for the faintest.

The 2-D fitting code GALFIT (Peng et al. 2002) was used to parameterize the UV emission. For each image we tested different combinations of point source and Sersic profiles, allowing the sky level, position and magnitudes of all components, as well the index and effective radii of the Sersic components, to vary. The final model was chosen according to the lowest χ^2 and best residuals (with the lowest number of components). The results are summarized in Table 2. Figure 11 show the UV image, GALFIT model and residuals for the nine objects. These will be discussed in detail in Section 4.

A Sersic profile (Sersic 1963, 1968; Graham & Driver 2005, for a review), $R^{1/n}$ is described by:

$$I(R) = I_e \exp \left[-b_n \left(\left(\frac{R}{R_e} \right)^{1/n} - 1 \right) \right] \quad (1)$$

where I_e is the intensity at the effective radius, R_e (distance that encloses half of the total emission), and b_n is a constant coupled to the value of n . Special cases of the Sersic profile are those where $n = 4$ (de Vaucouleurs profile), $n = 1$ (exponential profile) and $n = 0.5$ (Gaussian profile).

The TinyTim (Space Telescope Science Institute program to generate simulated HST point spread functions) models for the HRC PSF are not sufficient for our purposes. Instead, we used the *calibration plan* observations of Cycles 12 and 13 (programs 10054 and 10374). These programs contain observations of the spectrophotometric standard stars GD71, G191B2B, GD153 and HZ 14. To model our PSF, we compared the PSF created by each of these stars in each Cycle, as well as combinations of these. In general, the differences between each PSF are subtle and do not produce major differences in the models of the sources. However, the average PSF of the spectrophotometric stars of Cycle 13 produced better point source results (lower χ^2 and residuals) so we chose

to use it in our models. This PSF has a FWHM of ~ 1.9 pixels, implying a resolution of $\sim 0.05''$. However, the residuals for 1814+364 suggest that an even better PSF model is required (see Figure 11).

GALFIT yields the coordinates of the modeled components in pixels. The conversion to RA and Dec was performed using the astrometry information stored in the header of each HST/ACS -pipeline reduced- image (model errors are listed in Table 2). The radio positions of the sources are from the literature.

Unless otherwise noticed, all presented fluxes, luminosities and magnitudes are for the F330W filter passband, corrected for galactic extinction and k-correction. The magnitudes are in the STMAG system. Galactic extinction was corrected using the Galactic de-reddening curve in Cardelli et al. (1989) and the measured Galactic extinction values of Schlegel et al. (1998). K-correction (typically $\sim 0.1, 0.2$ magnitudes) and conversion of the literature (Allen et al. 2002) filters were done following the PEGASE (Fioc & Rocca-Volmerange 1997) templates of elliptical galaxies and using the IRAF package SYNPHOT. SYNPHOT was also used for measuring F330W magnitudes of the PEGASE and GALAXEV (Bruzual & Charlot 2003) stellar population models.

3. Nuclear and emission line contamination

Here we discuss several possible contributions to the near-UV light in these radio galaxies. Using ground-based, optical spectroscopy, Tadhunter et al. (2002) studied the nature of the UV excess in GPS, CSS and FR II sources at redshifts $0.15 < z < 0.7$. They found that the UV continuum in these sources has contributions from (1) nebular continuum, (2) direct AGN light, (3) scattered AGN light, and a (4) starburst component. The presence of possible emission line gas must be also considered.

The observed objects in our case are Narrow Line Radio Galaxies (NLRG) so we expect no contamination from direct light from the AGN. The main contribution from emission line gas to our observations would come from Mg II. It is usually only found in the nuclear Broad Line Region (BLR) of AGN hosts so we do not expect direct contamination from emission line gas.

To make a rough estimation of the extent of the possible contamination by direct light from the AGN, we use the STIS spectrum of 3C 277.1 (Labiano et al. 2005), a CSS QSO that could represent our worst case scenario: when we are looking into the nucleus. In 3C 277.1, all signs from nuclear contribution (broad lines and AGN continuum) and Mg II emission disappear at 0.8 kpc from the nucleus, roughly 1.5 times the FWHM of the PSF in the STIS observations. On average, 0.8 kpc correspond to $\sim 0.2''$ in our ACS observations and we could expect the nuclear traces to disappear closer to the center in our ACS galaxies. The C II] line is usually fainter than Mg II (Peterson 1997) in AGN (it is also not present in 3C 277.1) so it is unlikely that it is affecting our observations.

There are UV polarization observations of 1934–638 and 1345+125 but not for the rest of the sources so the presence of scattered nuclear light cannot be completely ruled out.

Table 1. Redshift and wavelengths.

Source	Catalogue	ID	Sample	Redshift	λ_{3100}	λ_{3300}	λ_{3700}	Emission lines
1117+146	4C 14.41	G	GPS	0.326	2338	2489	2790	C II] 2326, Mg II 2800
1233+418		G	CSS	0.25	2480	2640	2960	Mg II 2800
1345+125	4C 12.50	G	GPS	0.12174	2764	2942	3298	Mg II 2800
1443+77	3C 303.1	G	CSS	0.267	2447	2605	2920	C II] 2326, Mg II 2800
1607+268	CTD 093	G	GPS	0.473	2108	2240	2512	C II] 2326
1814-637		G	CSS	0.063	2916	3104	3481	[Ne V] 3426
1934-638		G	GPS	0.183	2620	2790	3128	Mg II 2800
1946+708		G	GPS	0.10083	2816	2998	3361	Mg II 2800
2352+495	DA 611	G	GPS	0.23790	2504	2666	2989	Mg II 2800

B1950 IAU and catalogue names, identification, GPS/CSS classification, redshift, rest-frame wavelengths covered by our observations and possible emission lines affecting our measurements. The throughput for HRC/F330W effectively covers $\sim 3100\text{\AA}$ to $\sim 3700\text{\AA}$. Columns 5 to 7 give the corresponding wavelengths of these limits and the maximum throughput of the filter in the rest frame of each source.

Tadhunter et al. (2002) find AGN scattered light in $\sim 37\%$ of their sample (including the GPS 1934–638), but in most cases it does not seem to dominate the UV emission. As we note below in Section 5.1, the UV light in the GPS sources tends not to be aligned with the radio source suggesting that it is not due to scattered nuclear light. Observations of 1345+125 by Hurt et al. (1999) are consistent with the existence of polarized UV light (though with large uncertainty). However, Tadhunter et al. (2005) found evidence of recent star formation and strong jet cloud interactions in 1345+125 (see also Holt et al. 2003; Surace et al. 1998).

In general, the contribution from nebular continuum in radio galaxies varies between 3 and 40% (Tadhunter et al. 2002). However, 3 out of the 4 CSS they studied are dominated by young stellar populations. Furthermore, for up to 50% of their sources (including GPS, CSS and FR II), the UV excess is dominated by young stellar populations. Similar results have been found for FR I and FR II sources at different redshifts (Aretxaga et al. 2001; Wills et al. 2002, 2004).

To sum up, the most probable sources of UV light in our images are star formation, scattered nuclear light and nebular continuum. However, it is likely that the contributions of the latter two are small.

4. UV morphology

We have modeled the UV emitting regions with GALFIT and found that all sources show at least two components, except 1117+146 (point source). The hosts of 1233+418, 1345+125, 1443+77, 1607+268, 1814–637 and 1934–638 show a combination of at least one Sersic¹ component (with different indices) and one or several point sources (see Table 2 and Figure 11). 1946+708 and 2352+495 show a combination of two and three point sources. In the near-IR, de Vries et al. (2000) find Sersic indices $2 \lesssim n \lesssim 5$ and effective radii $2 \text{ kpc} \lesssim R_e \lesssim 4 \text{ kpc}$ for GPS and CSS sources. Most of our data show point sources and/or Sersic profiles with indices $n \lesssim 2$ and radii $R_e \lesssim 400 \text{ parsec}$. The presence of these small clumps of near-UV emission is consistent with star forming regions in the host. Before addressing the nature of the UV emission, we describe the prop-

erties of this emission in relation to other properties, for the individual sample sources.

For our observations, the 3σ detection limit, for a point source (FWHM ~ 3 pixels) is 25.8 (no Galactic extinction applied). For comparison purposes with this limit and published data, the magnitudes listed in this section and Table 2 have not been corrected for Galactic extinction.

4.1. Notes on individual sources

1117+146: Identified as a GPS by O’Dea et al. (1991). The counterpart of the radio source corresponds to a $m_R=20.1$ galaxy (de Vries et al. 1995) at $z = 0.362$ (de Vries et al. 1998b). Radio observations (e.g., Fey & Charlot 1997) show a $\sim 100 \text{ mas}$ double radio source. Our image shows an unresolved 24.06 magnitude source.

1233+418: A CSS galaxy with a photometric R-band redshift $z_R = 0.25$ (Fanti et al. 2004). We detect a point source with magnitude 25.43. Our image (see Figure 11, first panel) suggests faint extended emission towards Northeast but the errors in the GALFIT model for this component are too large to be sure of its existence.

1345+125: 4C +12.50. A long known peaked spectrum radio source (e.g., Véron 1971). The counterpart of this GPS source is a $m_R=15.5$ galaxy (e.g., Stanghellini et al. 1993) at $z = 0.12174$ (Holt et al. 2003), in a cluster of fainter galaxies (Stanghellini et al. 1993). IR images of this well known ULIRG show an extremely reddened source with two nuclei separated $\sim 1.8''$ ($\sim 4 \text{ kpc}$) embedded in a common envelope and aligned roughly East-West (e.g., Scoville et al. 2000; Surace & Sanders 2000) suggesting an ongoing merger, which may have triggered the AGN (e.g., Heckman et al. 1986; Xiang et al. 2002). The western nucleus is the brightest and shows a Seyfert 2 spectrum (Gilmore & Shaw 1986). Veilleux et al. (1997) suggest that the source may have a hidden quasar, also supported by UV polarized continuum emission ($p=16.4\% \pm 2.6\%$, the polarization vector approximately perpendicular to the radio axis Hurt et al. 1999). VLBI imaging shows a complex, distorted $\sim 100 \text{ mas}$ ($\sim 0.2 \text{ kpc}$) source (e.g., Lister et al. 2003), roughly oriented North-South ($PA \sim -20 \text{ deg}$). Older observations of 1345+125 related the radio source to the East nucleus but improved astrometry showed that it is related to the western one (e.g. Stanghellini et al. 1997; Axon et al. 2000; Fanti 2000). Evans et al. (1999) study the molecular gas in 1345+125 and suggest that the molecular gas is fueling the AGN. Our UV image detects both nuclei separated by $\sim 1.8''$. The East component was modeled with a Sersic profile with index ~ 2.3 and an effective radius $\sim 0.3''$ and magnitude 21.84. The West nucleus shows a more complex structure: two Sersic profiles with magnitudes 21.14 and 21.20 and indices 1.6 and 0.33. This more complex structure could be due to interaction with the radio source. Optical emission line images (Axon et al. 2000; Batcheldor et al. 2006) show an arc of emission $\sim 1''$ North of the Western nucleus and fainter emission at $2''$. We do not detect UV emission associated with these emission line features. They also detect a faint tail of emission stretching from the West nucleus towards the

¹ The Sersic profiles are used to parameterize the data. It does not necessarily imply that these UV components are galaxies.

Table 2. Galfit components.

Source	Component	RA (J2000)	Dec (J2000)	STMAG	R_e (mas)	R_e (pc)	Index	Ratio
1117+146	Fey et al. (2004)	11:20:27.807 ±0.001	+14:20:54.99 ±0.02					
	Point source	11 20 27.7653 ±0.0001	14 20 54.33 ±0.06	24.06±0.06				
1233+418	Becker et al. (1995)	12:35:35.71 ±0.03	+41:37:07.40 ±0.32					
	Point source	12 35 35.6664 ±0.0004	+41:37:08.18 ±0.17	25.43±0.16				
	Sersic profile	12 35 35.677 ±0.001	+41 37 08.23 ±0.47	24.21±0.36	100±800	390±3100	0.04±0.6	0.06±0.09
1345+125	Ma et al. (1998)	13:47:33.3616	+12:17:24.240					
	Point source	13 47 33.3981 ±0.0001	+12 17 23.36 ±0.04	23.77±0.05				
	Sersic profile	13 47 33.3947 ±0.0002	+12 17 23.46 ±0.01	21.14±0.02	35 ±0.5	76±1	0.33±0.03	0.36±0.02
	Sersic profile	13 47 33.3950 ±0.0001	+12 17 23.41 ±0.06	21.20±0.04	108 ±7	234±15	1.62 ±0.13	0.76±0.03
1443+77	Sersic profile	13 47 33.5272 ±0.0003	+12 17 23.24 ±0.21	21.84±0.12	299 ±58	647±126	2.29±0.38	0.54±0.05
	Rengelink et al. (1997)	14:43:14.9±1.1	+77:07:28.6±3.8					
	Point source	14 43 14.666 ±0.001	+77 07 27.546 ±0.17	25.21 ±0.10				
	Point source	14 43 14.5832 ±0.0004	+77 07 27.702 ±0.06	24.06 ±0.06				
1607+268	Sersic profile	14 43 14.656 ±0.002	+77 07 27.430 ±0.10	20.36 ±0.16	1.1''±0.2''	4500±800	2.66±0.33	0.45±0.02
	Beasley et al. (2002)	16:09:13.3208	+26:41:29.036					
	Point source	16 09 13.2497 ±0.0002	+26 41 29.514 ±0.14	24.64 ±0.18				
	Sersic profile	16 09 13.2472 ±0.0002	+26 41 29.515 ±0.14	23.13 ±0.14	47±11	277±65	3.92±2.35	0.50±0.10
1814-637	Ma et al. (1998)	18:19:35.003 ±0.003	-63:45:48.194 ±0.01					
	Point source	18 19 35.3179 ±0.0001	-63 45 47.117 ±0.01	16.95±0.10				
	Sersic profile	18 19 35.3175 ±0.0001	-63 45 47.115 ±0.01	17.11 ±0.12	25±4	30±5	2.08±0.31	0.07±0.02
1934-638	Ma et al. (1998)	19:39:25.027 ±0.001	-63:42:45.626					
	Point source	19 39 25.0947 ±0.0009	-63 42 44.978 ±0.13	23.81±0.73				
	Sersic profile	19 39 25.0935 ±0.0001	-63 42 44.974 ±0.02	21.75±0.12	39±5	119±15	1.02±0.33	0.13±0.04
	Sersic profile	19 39 25.1032 ±0.0007	-63 42 45.037 ±0.06	21.08±0.07	354±45	1078±137	2.51±0.26	0.47±0.02
1946+708	Beasley et al. (2002)	19:45:53.5200 ±0.002	+70:55:48.732					
	Point source	19 45 53.299 ±0.002	+70 55 48.395 ±0.38	25.81±0.25				
	Point source	19 45 53.3016 ±0.0006	+70 55 48.476 ±0.12	24.59±0.09				
2352+495	Ma et al. (1998)	23:55:09.458 ±0.001	+49:50:08.340 ±0.01					
	Point source	23 55 09.4704 ±0.0004	+49 50.07.326 ±0.16	25.13±0.16				
	Point source	23 55 09.4634 ±0.0006	+49 50 07.507 ±0.25	25.53±0.19				
	Point source	23 55 09.4828 ±0.0003	+49 50 07.531 ±0.12	24.79±0.10				

The first line for each source corresponds to the most recent radio position, the rest of the lines correspond to the UV components of the GALFIT models. Errors not listed are smaller than 0.1 milliarcsec. The coordinates in the GALFIT models are from the HST coordinate system and correspond to the brightest pixel. The magnitudes are observed, not corrected from galactic extinction. R_e is the effective radius in milliarcsec except for 1443+77. Last two columns give the sersic indices and axial ratios.

west, present in our image and not modeled by GALFIT (see Figure 11). Surace et al. (1998) detect *compact blue knots* in 1345+125 around the source which they attribute to star forming regions. We detect the southern knots $\sim 2''$ south of the nuclei but not the northern one (see Figure 11).

1443+77: 3C 303.1. The optical counterpart of this CSS corresponds to a galaxy of $m_v \sim 20$ (e.g., Sanghera et al. 1995), at $z = 0.267$ (Kristian et al. 1978). The VLBI map (Sanghera et al. 1995) shows a $\sim 1.8''$ long (~ 7 kpc) double radio source aligned NW-SE (PA ~ 47 deg) aligned with the inner emission line gas (e.g. de Vries et al. 1999). XMM-Newton observations detect the ISM of the host galaxy as well as a second component which could be either Synchrotron Self Compton from the Southern radio lobe or hot gas shocked by the expansion of the radio source (O’Dea et al. 2006). The center of 1443+77 shows a complex structure in the optical, which could be due to an ongoing merger (e.g., de Vries et al. 1997; Axon et al. 2000) and it also shows up in our UV image. Axon et al. (2000) and de Vries et al. (1999) find an arc of emission south of the nucleus of the source and McCarthy et al. (1995) detects circumnuclear [O III] as far as $3''$ from the center. Our image suggests the presence of an arc of emission $\sim 0.9''$ (~ 4 kpc) from the nucleus. The integrated magnitude of this arc is ~ 23 . A region of the sky with the same area has a magnitude ~ 25 . The GALFIT model of the source consists of two

point sources of magnitudes 25.21 and 24.06, and a Sersic profile with index 2.66 and effective radius $1.1''$ (~ 4.5 kpc). The arc is not modeled by GALFIT so it is visible in the residuals of Figure 11. 1443+77 is the best candidate in our sample to be undergoing jet induced star formation (see below).

1607+268: Also known as CTD93. VLBI maps (e.g. Dallacasa et al. 1998) show a two-component, ~ 60 mas, GPS source. The counterpart is a galaxy at $z = 0.473$ (O’Dea et al. 1991) with $m_r = 20.4$ (Stanghellini et al. 1993). We observe a 24.64 magnitude point source on top of a 23.13 magnitude de Vaucouleurs component.

1814-637: VLBI imaging shows a two component CSS galaxy (e.g., Tzioumis et al. 2002). Although the radio source is small ($\sim 0.4''$, ~ 0.3 kpc) its radio spectrum does not peak at ~ 1 GHz. The optical identification corresponds to a $m_v=18.0$ galaxy at $z = 0.063$ (Wall & Peacock 1985). We observe a bright, 16.95 magnitude point source on top of a 17.11 magnitude Sersic profile with index $n \approx 2$. The UV object is ~ 2 arcsec to the Northeast of the radio source (Ma et al. 1998). At this redshift, $2'' \approx 2.4$ kpc so it is probably the counterpart.

1934-638: A long known GPS (Bolton et al. 1963). VLBI maps (e.g., Tzioumis et al. 1998) show two components separated by $\sim 40''$ (0.12 kpc at $z = 0.183$, Tadhunter et al. 1993). R-band and ISO observations (Jauncey et al. 1986; Fanti et al. 2000) show a system of two galaxies, separated by $\sim 3''$, con-

sistent with our observations. The GALFIT model yields two Sersic profiles of magnitudes 21.08 and 21.75 and a fainter point source with magnitude 23.81. 1934–638 shows significant polarization in the UV (3.5%, e.g., Tadhunter et al. 1994; Morganti et al. 1997), with the position angle of the electric vector perpendicular to the radio axis. Scattered AGN light probably makes a significant contribution to the UV excess in this source (Tadhunter et al. 2002). The polarization observations also suggest an anomalous environment (e.g., Fanti et al. 2000).

1946+708: The counterpart is identified with a $z = 0.10083$, $m_R = 16.3$ galaxy (e.g., Snellen et al. 2003). VLBI observations of this GPS source show an elongated, ~ 40 mas (~ 0.07 kpc) NE-SW structure (Taylor & Vermeulen 1997). Optical observations (Perlman et al. 2001) also suggest a NE-SW elongated source, consistent with the orientation of the two components in our GALFIT model: two point sources (aligned NE-SW) with magnitudes 24.59 and 25.81. Perlman et al. (2001) suggest that 1946+708 may be part of a group of galaxies and the closest would be $\sim 1'$ far from 1946+708. These objects fall outside our field and they have unknown redshifts.

2352+495: Snellen et al. (2003) identify the counterpart of this GPS source (e.g., O’Dea 1998) with a $z = 0.23790$, $m_R = 18.2$ galaxy. VLBI observations show a complex elongated $\sim 0.7''$ (~ 0.25 kpc) source oriented NW-SE (Pollack et al. 2003). Our ACS observations show three point sources in a circle about $0.5''$ wide, with magnitudes 24.79, 25.13 and 25.53.

5. UV and radio properties

Here we compare the UV and radio properties of our sample with those of a sample of 3CR FR I and FR II sources studied by Allen et al. (2002). The Allen et al. (2002) data consist of STIS near-UV-MAMA snapshots (exposure time of 1440 seconds) with filters F25SRF2 and F25CN182. The radio data have been collected from the papers listed in the individual notes above: O’Dea (1998), Morganti et al. (1993), Martel et al. (1999), Flesch & Hardcastle (2004) and the 3CRR on-line catalog (an update of the sample of Laing et al. 1983). The data are summarized in Table 3 and plotted in Figures 1 to 10.

We note that O’Dea & Baum (1997) found that the radio power of the bright GPS and CSS sample is independent of size and comparable to that of the most powerful FR II sources. However, the Allen et al. (2002) FR sources are low z 3CR, and therefore lower radio luminosity sources.

5.1. GPS sources

Most of the sources in our sample are very compact GPS sources, and therefore, are probably too small to strongly affect their environment on the scales resolved by these observations. However, some conclusions can be drawn from their integrated UV and radio properties.

Figure 1 suggests a trend between UV luminosity and radio power of GPS sources (consistent with the results of Raimann et al. 2005, for larger radio galaxies). This relationship could be produced by a larger reservoir of gas available

in the more luminous sources for fueling the radio source and supplying the starburst.

Inspection of Figure 2 shows that alignment between the UV and radio is found for sources ≥ 1 kpc, i.e., the compact GPS sources tend not to show systematic alignment. If the UV light was scattered nuclear light, it would be expected to align with the radio axis regardless of radio source size. The lack of alignment in the GPS sources suggests that the UV light is not scattered nuclear light. Instead, in the GPS sources, we may be detecting some clumps of star formation which are associated with the onset of the radio activity.

5.2. CSS sources

The fact that the GPS sources show UV emission on larger scales than the radio source and which are not aligned with the radio source is consistent with the hypothesis that the GPS sources are too small to strongly affect their environment on the scales resolved by these observations. In large scale 3CR sources, the jets extend far beyond the host galaxy. Therefore, if there is jet induced star formation, CSS sources are the best candidates to reveal it. We also note that the two brightest UV sources in our sample (1443+77 and 1814–637) are CSS.

Labiano et al. (2005) demonstrated the presence of gas ionized by the shocks from the expanding radio source in CSS sources. Furthermore, they found that 1443+77 shows the strongest contribution from shocks. We could also expect these shocks to be affecting the star formation in the host.

5.3. Is there jet-induced star formation?

Figure 3 suggests there is no correlation between UV luminosity and size of the radio source (i.e., the GPS, CSS and large 3CR sources have similar UV luminosities). Therefore, any UV emission which is related to source size does not seem to dominate the UV properties of the host. However, if the expansion of the radio lobes were enhancing the UV luminosity, it could have been unnoticed by our sample. The lack of a significant number of CSS sources in our sample (i.e. radio sizes comparable to the host) may cause us to be missing hosts with UV emission $\sim 10^9 L_\odot$.

If the jet is enhancing the star formation, we expect the radio source and UV emission to be aligned and have similar sizes. Sources with high UV luminosity (1443+77 and 1814–637) seem to show alignment between the UV and radio source (Figure 4). Observations of additional sources with sizes ≥ 1 kpc are needed to improve the statistics. Figure 5 shows that UV size and radio size are not correlated for most sources. However, two CSS and one GPS source (1443+77, 1814–637 and 2352+495) have similar UV and radio sizes. The radio source in 1233+418 is larger than the UV emission. However, the UV magnitudes for 1233+418 are close to the detection limit so we may be missing extended and fainter UV emission in this object.

Table 3 shows the position angles of the radio and UV in the GPS and CSS sources. We see that the CSS 1443+77 and

Table 3. UV and 5GHz radio properties.

Name	Type	Size _{5GHz}	UV Size	Log P _{5GHz}	Log(L/Lsun)	L _{UV} 10 ⁴⁰ (erg/s)	PA 5GHz	PA UV	Δ PA
1233+418	CSS	11.6	1.2	25.56	7.12±0.11	5.1±1.3	27	66	39
1443+77	CSS	6.9	8.1	25.86	8.66±0.06	180±25	140	116, 136, 20 ^a	4
1814–637	CSS	0.50	–	25.56	8.87±0.03	290±20	156	170	14
1117+146	GPS	0.40	0.2	26.41	7.45±0.02	11.0±0.5	120	–	–
1345+125	GPS	0.17	0.45	25.98	7.88±0.01	29.6±0.7	120, 26	165	45
1607+268	GPS	0.30	0.2	26.86	8.24±0.04	68±7	29	88	59
1934–638	GPS	0.13	0.5	26.65	8.24±0.03	68±5	88	140	52
1946+708	GPS	0.07	0.2	25.14	6.35±0.04	0.87±0.08	28	3	25
2352+495	GPS	0.86	0.9	26.23	7.39±0.03	9.6±0.7	153	157, 27, 85 ^b	4
3C 29	FR 1	133		24.99	7.63±0.12				
3C 35	FR 2	960		24.75	7.42±0.45				
3C 40	FR 2	20		24.12	7.56±0.13				
3C 66b	FR 1	300		24.45	7.78±0.25				
3C 192	FR 2	228		25.29	8.16±0.17				
3C 198	FR 2	512		24.79	8.80±0.08				
3C 227	FR 2	379		24.59	9.27±0.08				
3C 236	FR 2	4470		25.43	8.41±0.35				
3C 270	FR 1	55		23.74	7.43±0.06				
3C 285	FR 2	267		25.00	8.40±0.06				
3C 293	FR 1	225		24.91	8.38±0.06				
3C 296	FR 1	206		24.31	7.78±0.08				
3C 305	FR 1	11		24.59	8.37±0.09				
3C 310	FR 1	316		24.89	7.23±0.14				
3C 317	FR 1	18		24.37	7.91±0.12				
3C 321	FR 2	540		25.33	9.13±0.14				
3C 326	FR 2	1990		24.83	7.33±0.18				
3C 338	FR 1	68		23.96	7.56±0.04				
3C 353	FR 2	94		24.57	6.67±1.55				
3C 382	FR 2	204		25.19	10.35±0.22				
3C 388	FR 2	84		25.48	7.52±0.27				
3C 390.3	FR 2	246		25.47	9.44±0.22				
3C 405	FR 2	138		27.15	8.92±1.14				
3C 449	FR 1	514		23.93	7.98±0.51				
3C 465	FR 1	349		24.71	7.94±0.22				

UV luminosity for our GPS and CSS radio galaxies compared with large extended FR sources from Allen et al. (2002). Longest linear sizes are listed in kpc. Radio and UV position angles in degrees (from North to East) of each component. Difference in radio and UV PA of the most aligned components. The radio data are from O’Dea (1998), Morganti et al. (1993), Martel et al. (1999), Flesch & Hardcastle (2004) and the on-line 3CRR catalogue (Laing et al. 1983), measured at 5GHz.

^a The PA of the largest angular UV scale of 1345+125 is 130°.

^b The UV morphology of 2352+495 is a roughly equilateral triangle so no general PA for the complete source can be given (see Figure 11).

1814–637 and the GPS 1946+708 and 2352+495² are aligned with the UV. In addition 1443+77 1814–637 and 2352+495 have a ratio of radio to UV size of order unity (Figure 6). 1946+708 shows some alignment between the UV and radio components (~ 25 deg) but the radio source seems too small to have affected the UV in this host. The UV emission in 2352+495 has two components aligned with the radio source (and a third which is not aligned), but the unknown offset between radio and HST reference frames prevents us from accurately overlaying them. Therefore, 1443+77 and 1814–637 are currently the best candidates for jet induced star formation.

² For sources with several UV position angles, we use the most aligned component.

Figure 7 suggests a possible correlation between UV luminosity and the total spatial extent of the UV emission in GPS and CSS sources (we have checked that this trend is not dominated by 1443+77):

$$\log\left(\frac{L_{UV}}{L_{\odot}}\right) = (7.78 \pm 0.25) + (0.97 \pm 0.70) \times \log(\text{Size}_{UV})$$

This is consistent with the hypothesis that the UV emission is dominated by extended regions of star formation rather than by point-like AGN.

We also note several interesting null results. The detected UV luminosity in the GPS, CSS, and large 3CR sources is independent of redshift (out to $z=0.5$) (Figure 8). In the GPS and CSS sources, the alignment does not depend on either radio power (Figure 9) or redshift (Figure 10); though in both cases

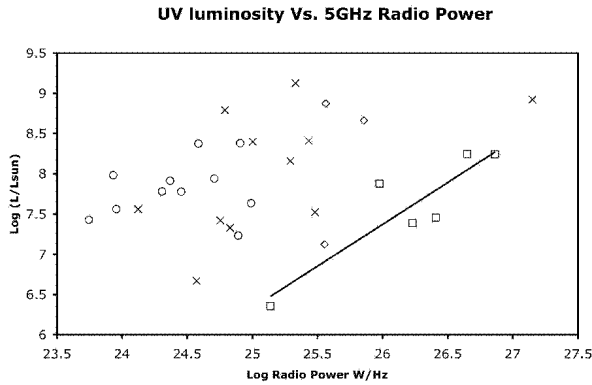


Fig. 1. UV luminosity and radio power of the combined sample of GPS/CSS and FR I, FR II from Allen et al. (2002). The solid line shows the correlation between UV luminosity and radio power for GPS sources.

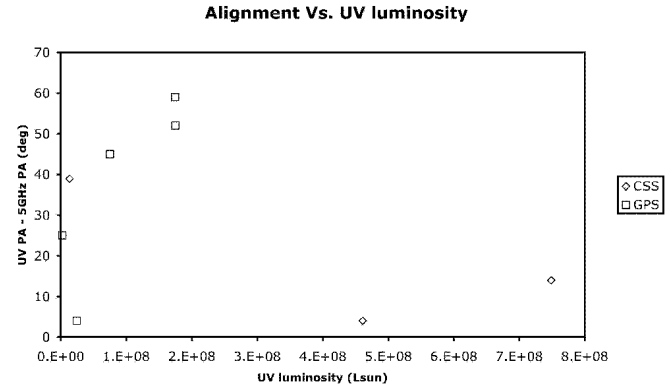


Fig. 4. As Figure 2, for UV luminosity.

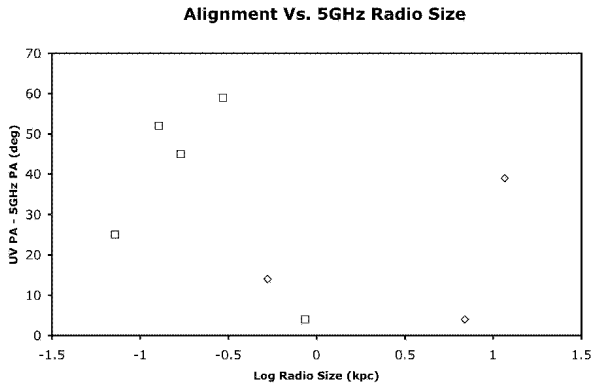


Fig. 2. Difference between the UV and radio position angles (alignment) of the GPS and CSS galaxies versus radio size.

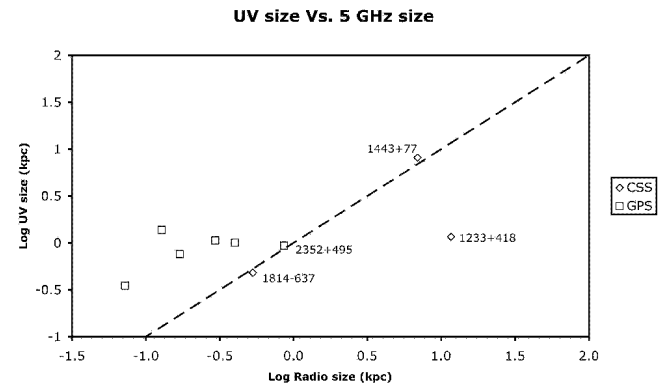


Fig. 5. UV size and radio size of GPS and CSS sources. The dashed line marks the locus of sources with equal radio and UV sizes.

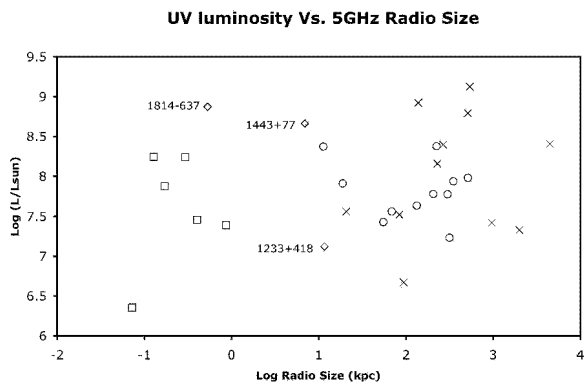


Fig. 3. As Figure 1, for radio size.

the statistics are dominated by the GPS sources which seem not to show alignment on the scales resolved by these observations.

6. Stellar synthesis models

GPS and CSS sources are usually associated with massive ellipticals of ages ~ 5 Gyr and solar metallicities

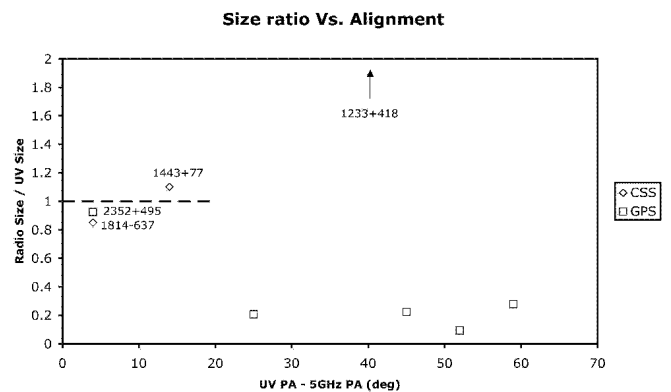


Fig. 6. Ratio of radio and UV sizes versus the alignment of the GPS and CSS sources. The dashed line marks the locus for sources with same UV and radio size and highest alignment i.e. where the radio source is most likely affecting the star formation in the host. The point for 1233+418 lies outside the plot (represented by the arrow).

(e.g., de Vries et al. 2000, 1998a). With this assumptions, we use stellar population synthesis models by Bruzual & Charlot (2003) using the Chabrier (Chabrier 2003) initial mass function and Padova evolutionary tracks, for a 1 Myr long burst of star formation and a delta single burst model for popula-

Table 4. Mass from luminosity.

Name	GALAXEV LB		GALAXEV DB		PEGASE		Average
	10 Gyr	1 Gyr	10 Gyr	1 Gyr	10 Gyr	1 Gyr	
1117+146	2.2×10^{11}	2.1×10^8	2.3×10^{11}	5.5×10^9	2.6×10^{10}	8.2×10^8	8.0×10^{10}
1233+418	5.2×10^{10}	1.0×10^8	5.6×10^{10}	1.8×10^9	1.1×10^{10}	3.9×10^8	2.0×10^{10}
1345+125	1.2×10^{11}	6.7×10^8	1.2×10^{11}	6.0×10^9	4.7×10^{10}	2.2×10^9	4.9×10^{10}
1443+77	2.0×10^{12}	3.3×10^9	2.2×10^{12}	6.2×10^{10}	3.7×10^{11}	1.3×10^{10}	7.7×10^{11}
1607+268	1.9×10^{12}	1.1×10^9	1.9×10^{12}	3.2×10^{10}	1.5×10^{11}	4.3×10^9	6.6×10^{11}
1814-63	1.1×10^{13}	4.6×10^9	1.1×10^{13}	2.0×10^{11}	7.1×10^{11}	2.0×10^{10}	3.8×10^{12}
1934-638	3.0×10^{11}	1.1×10^9	3.3×10^{11}	1.3×10^{10}	9.5×10^{10}	3.9×10^9	1.2×10^{11}
1946+708	1.4×10^9	9.6×10^6	1.5×10^9	7.8×10^7	6.2×10^8	3.1×10^7	6.1×10^8
2352+495	4.1×10^{10}	9.0×10^7	4.4×10^{10}	1.5×10^9	9.3×10^9	3.4×10^8	1.6×10^{10}
Average	1.7×10^{12}	1.2×10^9	1.8×10^{12}	3.6×10^{10}	1.6×10^{11}	4.9×10^9	6.1×10^{11}
Name	10 Myr		1 Myr		Average		Average
	10 Myr	1 Myr	10 Myr	1 Myr	10 Myr	1 Myr	
1117+146	1.7×10^9	1.8×10^8	1.4×10^6	4.4×10^6	5.9×10^7	2.5×10^8	3.7×10^8
1233+418	1.0×10^9	1.0×10^8	8.3×10^5	2.5×10^6	3.7×10^7	1.8×10^8	2.3×10^8
1345+125	8.9×10^9	8.2×10^8	7.1×10^6	2.0×10^7	3.0×10^8	1.4×10^9	1.9×10^9
1443+77	3.2×10^{10}	3.1×10^9	2.5×10^7	7.8×10^7	1.1×10^9	5.4×10^9	7.0×10^9
1607+268	8.1×10^9	8.3×10^8	6.4×10^6	2.2×10^7	2.8×10^8	1.2×10^9	1.7×10^9
1814-63	3.2×10^{10}	3.5×10^9	2.6×10^7	9.5×10^7	1.3×10^9	6.1×10^9	7.2×10^9
1934-638	1.3×10^{10}	1.2×10^9	1.0×10^7	3.0×10^7	4.4×10^8	2.1×10^9	2.8×10^9
1946+708	1.3×10^8	1.2×10^7	1.1×10^5	3.0×10^5	4.4×10^6	2.1×10^7	2.9×10^7
2352+495	9.4×10^8	9.1×10^7	7.5×10^5	2.3×10^6	3.3×10^7	1.6×10^8	2.0×10^8
Average	1.1×10^{10}	1.1×10^9	8.7×10^6	2.8×10^7	3.9×10^8	1.9×10^9	2.4×10^9

Mass in M_{\odot} needed to reproduce the observed F330W luminosity, according to the mass to luminosity ratio from each model. LB is the 1 Myr long burst, DB is the delta single burst model, PEGASE is the elliptical template model. The table is divided two halves corresponding to models of Gyr and Myr. Last column and last line of each block give the average mass for each source and model.

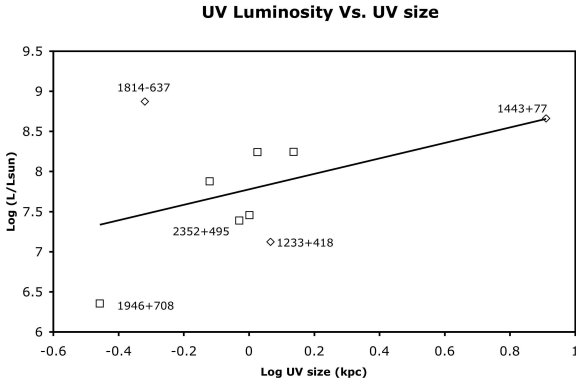


Fig. 7. As Figure 1, for UV size. The trend is similar with or without 1443+077.

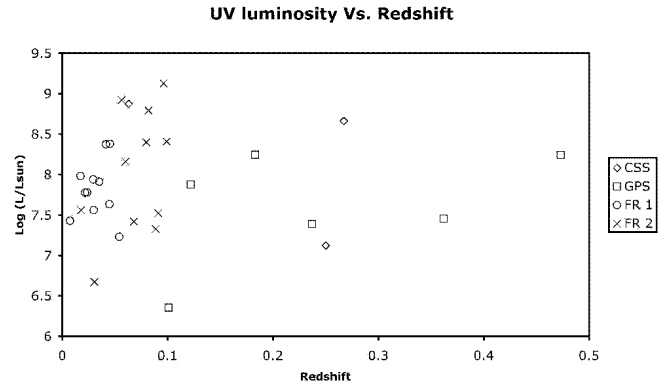


Fig. 8. As Figure 1, for redshift.

tions of 10^4 , 10^3 , 10 and 1 Myr to compare our UV luminosity measurements and to estimate the mass and age of stars producing the UV emission in our sources (Table 4). We also compare the measurements with the elliptical galaxy templates from PEGASE.

Inspection of Table 4 shows that our observations are generally consistent with models of a single instantaneous burst of $10^6 - 10^7 M_{\odot}$, $\lesssim 10$ Myr ago. However, some sources may be dominated by intermediate-age (0.1 to 1 Gyr) populations (with masses $\sim 10^9 M_{\odot}$, e.g., Tadhunter et al. 2005). These young and intermediate ages in our GPS/CSS sources are also consistent with stellar population ages measured in hosts of powerful radio galaxies (Raimann et al. 2005) and other CSS sources

(e.g., Johnston et al. 2005). The models which require old and massive stellar populations to produce the UV light are inconsistent with the small measured sizes for the UV emitting regions.

Our observations are consistent with a scenario in which a single event is responsible for triggering the AGN and initiating a starburst. However, the dynamical ages of GPS and CSS sources are much smaller (between 10^3 and 10^6 (e.g., Polatidis & Conway 2003; O’Dea 1998)) than the estimated ages of the stellar populations produced in the starburst. This implies a minimum time delay between the start of the starburst and the start of the radio activity of 10 Myr. The delay could be as long as 1 Gyr if the 1 Gyr stellar population models are

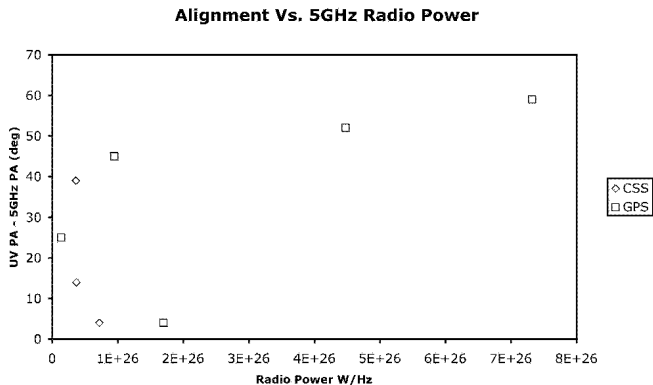


Fig. 9. As Figure 2, for radio power.

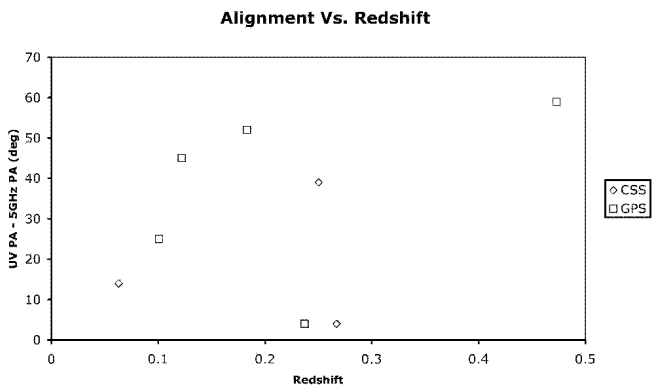


Fig. 10. As Figure 2, for redshift.

correct. The apparent delay between starburst and formation of the radio source has been found in objects with possible connections between the starburst and the formation of the AGN and radio source (Raimann et al. 2005; Tadhunter et al. 2005) and is predicted by theoretical calculations of the time needed for the gas to reach the center of the galaxy after a tidal interaction (e.g., Lin et al. 1988).

7. Summary

We have obtained HST/ACS/HRC near-UV high resolution images of compact GPS and CSS radio galaxies which are likely to be the young progenitors of large scale powerful radio galaxies. We detect near-UV emission in point sources and/or small clumps (tens to hundreds of pc scale) in eight of the sources, consistent with the presence of recent star formation. The UV luminosity in the GPS and CSS sources is similar to that measured in nearby large 3CR radio galaxies by Allen et al. (2002). In the GPS sources as a whole we do not see systematic alignment between the radio and UV. This may be because the GPS radio sources are smaller than the scales resolved by these HST observations. The lack of alignment in the GPS sources implies that the UV emission is not due to scattered nuclear light.

There is evidence for a correlation between radio and UV luminosity in the GPS sources. This relationship could be pro-

duced by having a larger reservoir of gas available in the more luminous sources for fueling the radio source and supplying the starburst.

In two CSS sources, 1443+77 and 1814-637 the near-UV emission is aligned with and co-spatial with the the radio emission and we suggest that star formation has been triggered or at least enhanced by expansion of the radio source through the host.

We suggest that the starburst and AGN are triggered by the same event. Comparison with stellar population synthesis models suggests the data are consistent with star formation occurring in a burst $\lesssim 10$ Myr ago (though models as old as 1 Gyr are not ruled out). The radio source ages are much smaller (e.g., 10^3 to 10^6 yr) suggesting that there is a minimum delay of 10 Myr between the onset of the starburst and the onset of the radio activity (see also Raimann et al. 2005; Tadhunter et al. 2005). Observations at other wavelengths and measurement of the colors are needed to further asses the nature of the observed UV properties.

G

Acknowledgements. AL wishes to thank Dr. Peng (STScI) for his help with GALFIT and Dr. I.A.G. Snellen (Leiden) for fruitful scientific discussions. WDV's work was performed under the auspices of the U.S. Department of Energy, National Nuclear Security Administration by the University of California, Lawrence Livermore National Laboratory under contract No. W-7405-Eng-48. This research has made use of NASA's Astrophysics Data System Bibliographic Services and of the NASA/IPAC Extragalactic Database (NED) which is operated by the Jet Propulsion Laboratory, California Institute of Technology, under contract with the National Aeronautics and Space Administration. This research is based on observations made with the NASA/ESA Hubble Space Telescope, obtained from the data archive at the Space Telescope Institute. STScI is operated by the association of Universities for Research in Astronomy, Inc. under the NASA contract NAS 5-26555.

References

- Allen, M. G., Sparks, W. B., Koekemoer, A., et al. 2002, *ApJS*, 139, 411
- Aretxaga, I., Terlevich, E., Terlevich, R. J., Cotter, G., & Díaz, Á. I. 2001, *MNRAS*, 325, 636
- Axon, D. J., Capetti, A., Fanti, R., et al. 2000, *AJ*, 120, 2284
- Batcheldor, D., Tadhunter, C., Holt, J., et al. 2006, in preparation
- Baum, S. A., Heckman, T. M., & van Breugel, W. 1992, *ApJ*, 389, 208
- Beasley, A. J., Gordon, D., Peck, A. B., et al. 2002, *ApJS*, 141, 13
- Becker, R. H., White, R. L., & Helfand, D. J. 1995, *ApJ*, 450, 559
- Bolton, J. G., Gardner, F. F., & Mackey, F. B. 1963, *Nature*, 199, 682
- Bruzual, G. & Charlot, S. 2003, *MNRAS*, 344, 1000
- Cardelli, J. A., Clayton, G. C., & Mathis, J. S. 1989, *ApJ*, 345, 245
- Chabrier, G. 2003, *PASP*, 115, 763
- Chiaberge, M., Macchetto, F. D., Sparks, W. B., et al. 2002, *ApJ*, 571, 247

- Dallacasa, D., Bondi, M., Alef, W., & Mantovani, F. 1998, *A&AS*, 129, 219
- de Vries, W. H., Barthel, P. D., & Hes, R. 1995, *A&AS*, 114, 259
- de Vries, W. H., O’Dea, C. P., Barthel, P. D., et al. 2000, *AJ*, 120, 2300
- de Vries, W. H., O’Dea, C. P., Baum, S. A., & Barthel, P. D. 1999, *ApJ*, 526, 27
- de Vries, W. H., O’Dea, C. P., Baum, S. A., et al. 1998a, *ApJ*, 503, 156
- de Vries, W. H., O’Dea, C. P., Baum, S. A., et al. 1997, *ApJS*, 110, 191
- de Vries, W. H., O’Dea, C. P., Perlman, E., et al. 1998b, *ApJ*, 503, 138
- Evans, A. S., Kim, D. C., Mazzarella, J. M., Scoville, N. Z., & Sanders, D. B. 1999, *ApJ*, 521, L107
- Fanti, C. 2000, in *EVN Symposium 2000, Proceedings of the 5th european VLBI Network Symposium held at Chalmers University of Technology, Gothenburg, Sweden, June 29 - July 1, 2000*, Eds.: J.E. Conway, A.G. Polatidis, R.S. Booth and Y.M. Pihlström, published by Onsala Space Observatory, p. 73
- Fanti, C., Branchesi, M., Cotton, W. D., et al. 2004, *A&A*, 427, 465
- Fanti, C., Pozzi, F., Dallacasa, D., et al. 2001, *A&A*, 369, 380
- Fanti, C., Pozzi, F., Fanti, R., et al. 2000, *A&A*, 358, 499
- Fanti, R., Fanti, C., Schilizzi, R. T., et al. 1990, *A&A*, 231, 333
- Fey, A. L. & Charlot, P. 1997, *ApJS*, 111, 95
- Fey, A. L., Ma, C., Arias, E. F., et al. 2004, *AJ*, 127, 3587
- Fioc, M. & Rocca-Volmerange, B. 1997, *A&A*, 326, 950
- Flesch, E. & Hardcastle, M. J. 2004, *A&A*, 427, 387
- Gebhardt, K., Bender, R., Bower, G., et al. 2000, *ApJ*, 539, L13
- Gilmore, G. & Shaw, M. A. 1986, *Nature*, 321, 750
- Graham, A. W. & Driver, S. P. 2005, *Publications of the Astronomical Society of Australia*, 22, 118
- Heckman, T. M., Smith, E. P., Baum, S. A., et al. 1986, *ApJ*, 311, 526
- Ho, L. C. 2005, *ArXiv Astrophysics e-prints*, astro-ph/0511157
- Holt, J., Tadhunter, C. N., & Morganti, R. 2003, *MNRAS*, 342, 227
- Hurt, T., Antonucci, R., Cohen, R., Kinney, A., & Krolik, J. 1999, *ApJ*, 514, 579
- Israel, F. P. 1998, *A&A Rev.*, 8, 237
- Jauncey, D. L., White, G. L., Batty, M. J., & Preston, R. A. 1986, *AJ*, 92, 1036
- Johnston, H. M., Hunstead, R. W., Cotter, G., & Sadler, E. M. 2005, *MNRAS*, 356, 515
- Koekemoer, A. M., Fruchter, A. S., Hook, R. N., & Hack, W. 2002, in *The 2002 HST Calibration Workshop : Hubble after the Installation of the ACS and the NICMOS Cooling System*, Proceedings of a Workshop held at the Space Telescope Science Institute, Baltimore, Maryland, October 17 and 18, 2002. Edited by Santiago Arribas, Anton Koekemoer, and Brad Whitmore. Baltimore, MD: Space Telescope Science Institute, 2002, p. 339
- Koekemoer, A. M., O’Dea, C. P., Sarazin, C. L., et al. 1999, *ApJ*, 525, 621
- Kristian, J., Sandage, A., & Katem, B. 1978, *ApJ*, 219, 803
- Labiano, A., O’Dea, C. P., Gelderman, R., et al. 2005, *A&A*, 436, 493
- Laing, R. A., Riley, J. M., & Longair, M. S. 1983, *MNRAS*, 204, 151
- Lin, D. N. C., Pringle, J. E., & Rees, M. J. 1988, *ApJ*, 328, 103
- Lister, M. L., Kellermann, K. I., Vermeulen, R. C., et al. 2003, *ApJ*, 584, 135
- Ma, C., Arias, E. F., Eubanks, T. M., et al. 1998, *AJ*, 116, 516
- Martel, A. R., Baum, S. A., Sparks, W. B., et al. 1999, *ApJS*, 122, 81
- Martel, A. R., Sparks, W. B., Allen, M. G., Koekemoer, A. M., & Baum, S. A. 2002, *AJ*, 123, 1357
- McCarthy, P. J., Spinrad, H., & van Breugel, W. 1995, *ApJS*, 99, 27
- Mellema, G., Kurk, J. D., & Röttgering, H. J. A. 2002, *A&A*, 395, L13
- Morganti, R., Killeen, N. E. B., & Tadhunter, C. N. 1993, *MNRAS*, 263, 1023
- Morganti, R., Tadhunter, C. N., Dickson, R., & Shaw, M. 1997, *A&A*, 326, 130
- O’Dea, C., Mu, B., Worrall, D., et al. 2006, *astro-ph/0608320*
- O’Dea, C. P. 1998, *PASP*, 110, 493
- O’Dea, C. P. & Baum, S. A. 1997, *AJ*, 113, 148
- O’Dea, C. P., Baum, S. A., & Stanghellini, C. 1991, *ApJ*, 380, 66
- O’Dea, C. P., de Vries, W. H., Koekemoer, A. M., et al. 2003, *Publications of the Astronomical Society of Australia*, 20, 88
- O’Dea, C. P., Koekemoer, A. M., Baum, S. A., et al. 2001, *AJ*, 121, 1915
- Peng, C. Y., Ho, L. C., Impey, C. D., & Rix, H.-W. 2002, *AJ*, 124, 266
- Perlman, E. S., Stocke, J. T., Conway, J., & Reynolds, C. 2001, *AJ*, 122, 536
- Peterson, B. M., ed. 1997, *An introduction to active galactic nuclei* (Cambridge, New York: Cambridge University Press)
- Polatidis, A. G. & Conway, J. E. 2003, *Publications of the Astronomical Society of Australia*, 20, 69
- Pollack, L. K., Taylor, G. B., & Zavala, R. T. 2003, *ApJ*, 589, 733
- Raimann, D., Storchi-Bergmann, T., Quintana, H., Hunstead, R., & Wisotzki, L. 2005, *MNRAS*, 1022
- Rees, M. J. 1989, *MNRAS*, 239, 1P
- Rengelink, R. B., Tang, Y., de Bruyn, A. G., et al. 1997, *A&AS*, 124, 259
- Sanghera, H. S., Saikia, D. J., Ludke, E., et al. 1995, *A&A*, 295, 629
- Schlegel, D. J., Finkbeiner, D. P., & Davis, M. 1998, *ApJ*, 500, 525
- Scoville, N. Z., Evans, A. S., Thompson, R., et al. 2000, *AJ*, 119, 991
- Sersic, J. L. 1963, *Boletin de la Asociacion Argentina de Astronomia La Plata Argentina*, 6, 41
- Sersic, J. L. 1968, *Atlas de galaxias australes* (Cordoba, Argentina: Observatorio Astronomico, 1968)
- Snellen, I. A. G., Lehnert, M. D., Bremer, M. N., & Schilizzi, R. T. 2003, *MNRAS*, 342, 889
- Stanghellini, C. 1992, *PhD Thesis*, University of Bologna

- Stanghellini, C., O’Dea, C. P., Baum, S. A., et al. 1997, *A&A*, 325, 943 ‘1233+418’ on page 3
 ‘1345+125’ on page 3
 Stanghellini, C., O’Dea, C. P., Baum, S. A., & Laurikainen, E. 1993, *ApJS*, 88, 1 ‘4C 12.50’ on page 3
 ‘1443+77’ on page 3
 Surace, J. A. & Sanders, D. B. 2000, *AJ*, 120, 604 ‘3C 303.1’ on page 3
 Surace, J. A., Sanders, D. B., Vacca, W. D., Veilleux, S., & Mazzarella, J. M. 1998, *ApJ*, 492, 116 ‘1607+268’ on page 3
 ‘CTD 093’ on page 3
 Tadhunter, C., Dickson, R., Morganti, R., et al. 2002, *MNRAS*, 330, 977 ‘1814–637’ on page 3
 ‘1934–638’ on page 3
 Tadhunter, C., Robinson, T. G., González Delgado, R. M., Wills, K., & Morganti, R. 2005, *MNRAS*, 356, 480 ‘1946+708’ on page 3
 ‘2352+495’ on page 3
 Tadhunter, C. N., Morganti, R., di Serego-Alighieri, S., Fosbury, R. A. E., & Danziger, I. J. 1993, *MNRAS*, 263, 999 ‘DA 611’ on page 3
 ‘1934–638’ on page 3
 ‘1345+125’ on page 3
 Tadhunter, C. N., Shaw, M. A., & Morganti, R. 1994, *MNRAS*, 271, 807 ‘1345+125’ on page 3
 ‘1117+146’ on page 3
 Taylor, G. B. & Vermeulen, R. C. 1997, *ApJ*, 485, L9+ ‘1233+418’ on page 3
 Tzioumis, A., King, E., Morganti, R., et al. 2002, *A&A*, 392, 841 ‘1345+125’ on page 3
 ‘1443+77’ on page 3
 Tzioumis, A. K., King, E. A., Reynolds, J. E., et al. 1998, in *ASP Conf. Ser. 144: IAU Colloq. 164: Radio Emission from Galactic and Extragalactic Compact Sources*, 179 ‘1607+268’ on page 3
 ‘1814–637’ on page 3
 ‘1934–638’ on page 3
 Véron, M. P. 1971, *A&A*, 11, 1 ‘1946+708’ on page 3
 Veilleux, S., Sanders, D. B., & Kim, D.-C. 1997, *ApJ*, 484, 92 ‘2352+495’ on page 3
 Wall, J. V. & Peacock, J. A. 1985, *MNRAS*, 216, 173 ‘1117+146’ on page 3
 Wills, K. A., Morganti, R., Tadhunter, C. N., Robinson, T. G., & Villar-Martin, M. 2004, *MNRAS*, 347, 771 ‘1233+418’ on page 3
 ‘1345+125’ on page 3
 Wills, K. A., Tadhunter, C. N., Robinson, T. G., & Morganti, R. 2002, *MNRAS*, 333, 211 ‘4C +12.50’ on page 3
 ‘1345+125’ on page 3
 Xiang, L., Stanghellini, C., Dallacasa, D., & Haiyan, Z. 2002, *A&A*, 385, 768 ‘1345+125’ on page 3
 ‘1117+146’ on page 4
 ‘1233+418’ on page 4
 ‘1345+125’ on page 4
 ‘1443+77’ on page 4
 ‘1607+268’ on page 4
 ‘1814–637’ on page 4
 ‘1934–638’ on page 4
 ‘1946+708’ on page 4
 ‘2352+495’ on page 4
 ‘1443+77’ on page 4
 ‘1345+125’ on page 4
 ‘1443+77’ on page 4
 ‘3C 303.1’ on page 4
 ‘1443+77’ on page 4
 ‘1607+268’ on page 4
 ‘1814–637’ on page 4
 ‘1934–638’ on page 4
 ‘1934–638’ on page 5
 ‘1946+708’ on page 5
 ‘1946+708’ on page 5
 ‘1946+708’ on page 5
 ‘2352+495’ on page 5
 ‘1443+77’ on page 5
 ‘1814–637’ on page 5
 ‘1443+77’ on page 5
 ‘1443+77’ on page 5
 ‘1814–637’ on page 5

List of Objects

- ‘1443+77’ on page 1
 ‘1814–637’ on page 1
 ‘1117+146’ on page 2
 ‘1233+418’ on page 2
 ‘1345+125’ on page 2
 ‘1443+77’ on page 2
 ‘1607+268’ on page 2
 ‘1814–637’ on page 2
 ‘1934–638’ on page 2
 ‘1946+708’ on page 2
 ‘2352+495’ on page 2
 ‘GD71’ on page 2
 ‘G191B2B’ on page 2
 ‘GD153’ on page 2
 ‘HZ 14’ on page 2
 ‘1814+364’ on page 2
 ‘3C 277.1’ on page 2
 ‘3C 277.1’ on page 2
 ‘3C 277.1’ on page 2
 ‘1934–638’ on page 2
 ‘1345+125’ on page 2
 ‘1117+146’ on page 3
 ‘4C 14.41’ on page 3

'1443+77' on page 5	'1607+268' on page 8
'1814-637' on page 5	'1814-63' on page 8
'2352+495' on page 5	'1934-638' on page 8
'1233+418' on page 5	'1946+708' on page 8
'1233+418' on page 5	'2352+495' on page 8
'1443+77' on page 5	'1117+146' on page 8
'1233+418' on page 6	'1233+418' on page 8
'1443+77' on page 6	'1345+125' on page 8
'1814-637' on page 6	'1443+77' on page 8
'1117+146' on page 6	'1607+268' on page 8
'1345+125' on page 6	'1814-63' on page 8
'1607+268' on page 6	'1934-638' on page 8
'1934-638' on page 6	'1946+708' on page 8
'1946+708' on page 6	'2352+495' on page 8
'2352+495' on page 6	'1443+077' on page 8
'3C 29' on page 6	'1443+77' on page 9
'3C 35' on page 6	'1814-637' on page 9
'3C 40' on page 6	
'3C 66b' on page 6	
'3C 192' on page 6	
'3C 198' on page 6	
'3C 227' on page 6	
'3C 236' on page 6	
'3C 270' on page 6	
'3C 285' on page 6	
'3C 293' on page 6	
'3C 296' on page 6	
'3C 305' on page 6	
'3C 310' on page 6	
'3C 317' on page 6	
'3C 321' on page 6	
'3C 326' on page 6	
'3C 338' on page 6	
'3C 353' on page 6	
'3C 382' on page 6	
'3C 388' on page 6	
'3C 390.3' on page 6	
'3C 405' on page 6	
'3C 449' on page 6	
'3C 465' on page 6	
'1345+125' on page 6	
'2352+495' on page 6	
'1814-637' on page 6	
'1946+708' on page 6	
'2352+495' on page 6	
'1443+77' on page 6	
'1814-637' on page 6	
'2352+495' on page 6	
'1946+708' on page 6	
'2352+495' on page 6	
'1443+77' on page 6	
'1814-637' on page 6	
'1443+77' on page 6	
'1233+418' on page 7	
'1117+146' on page 8	
'1233+418' on page 8	
'1345+125' on page 8	
'1443+77' on page 8	

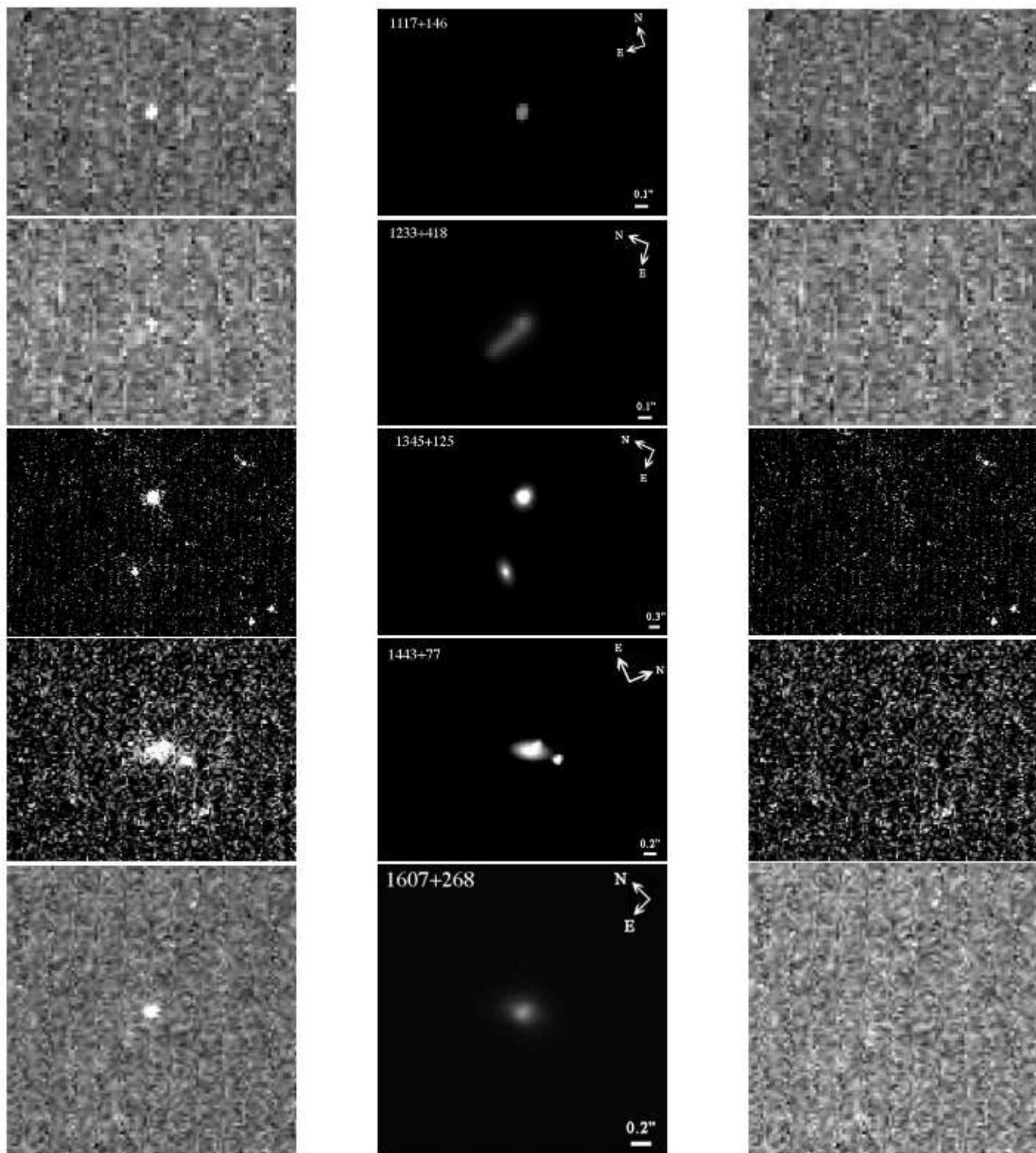


Fig. 11. ACS HRC F330W image (left panels), GALFIT model (center panels) and residuals (right panels) of our sample.

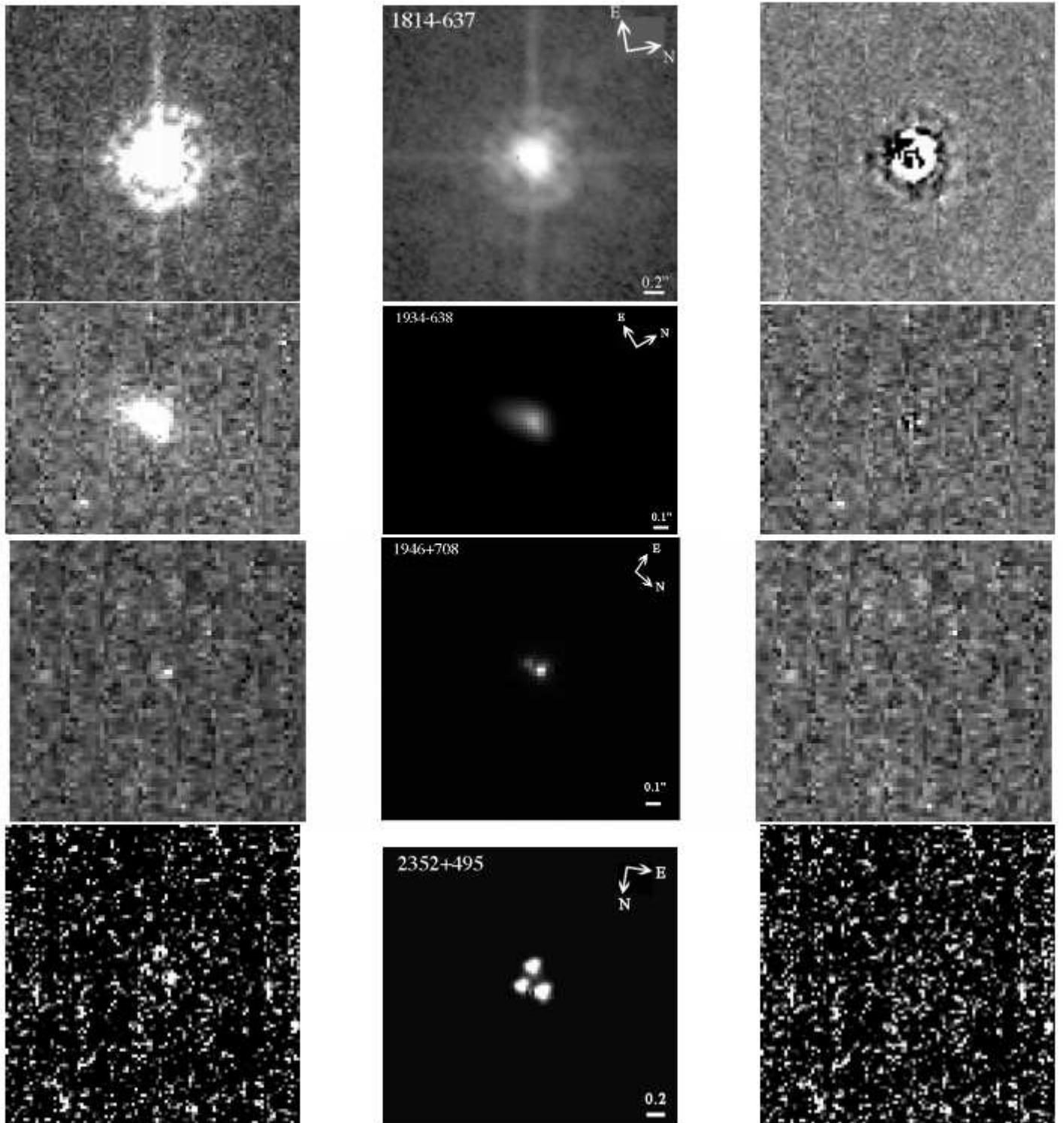


Fig. 11. Continued.